Supplementary Information

A highly effective fabrication of two dimensional metal oxides as high performances lithium storage anodes

Zhi Chen[a,1], Cun Wang[a,1], Min Chen[a], Changchun Ye[a], Zeheng Lin[a], Lidan Xing[a,b], Youhao Liao[a,b], Mengqing Xu[a,b], Guozhong Cao[c,*], Weishan Li[a,b,*]

[a] School of Chemistry and Environment, South China Normal University, Guangzhou 510631, China

[b] Engineering Research Center of MTEES (Ministry of Education), Research Center of BMET (Guangdong Province), Engineering Lab. of OFMHEB (Guangdong Province), Key Lab. of ETESPG (GHEI), and Innovative Platform for ITBMD (Guangzhou Municipality), South China Normal University, Guangzhou 510006, China

[c] Department of Materials Science and Engineering, University of Washington, Seattle, Washington 98195, United States.

* Corresponding authors, email: gzcao@u.washington.edu; liwsh@scnu.edu.cn.

1 These authors contributed equally to this work.

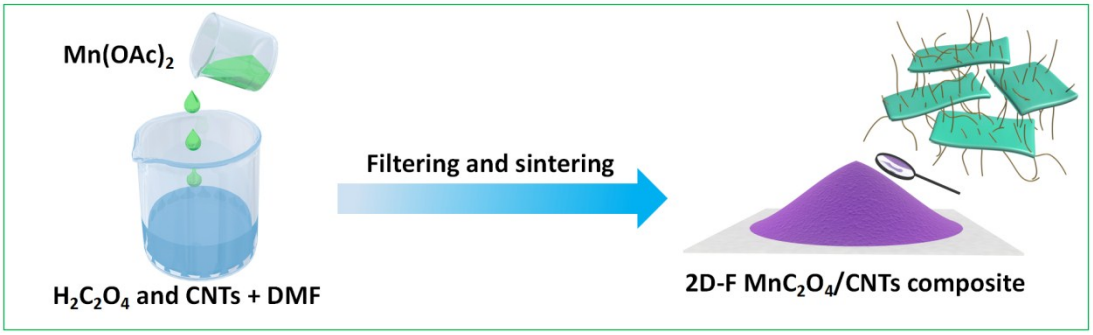

Figure S1. Schematic formation process of 2D-F MnC_2O_4/CNTs composite.

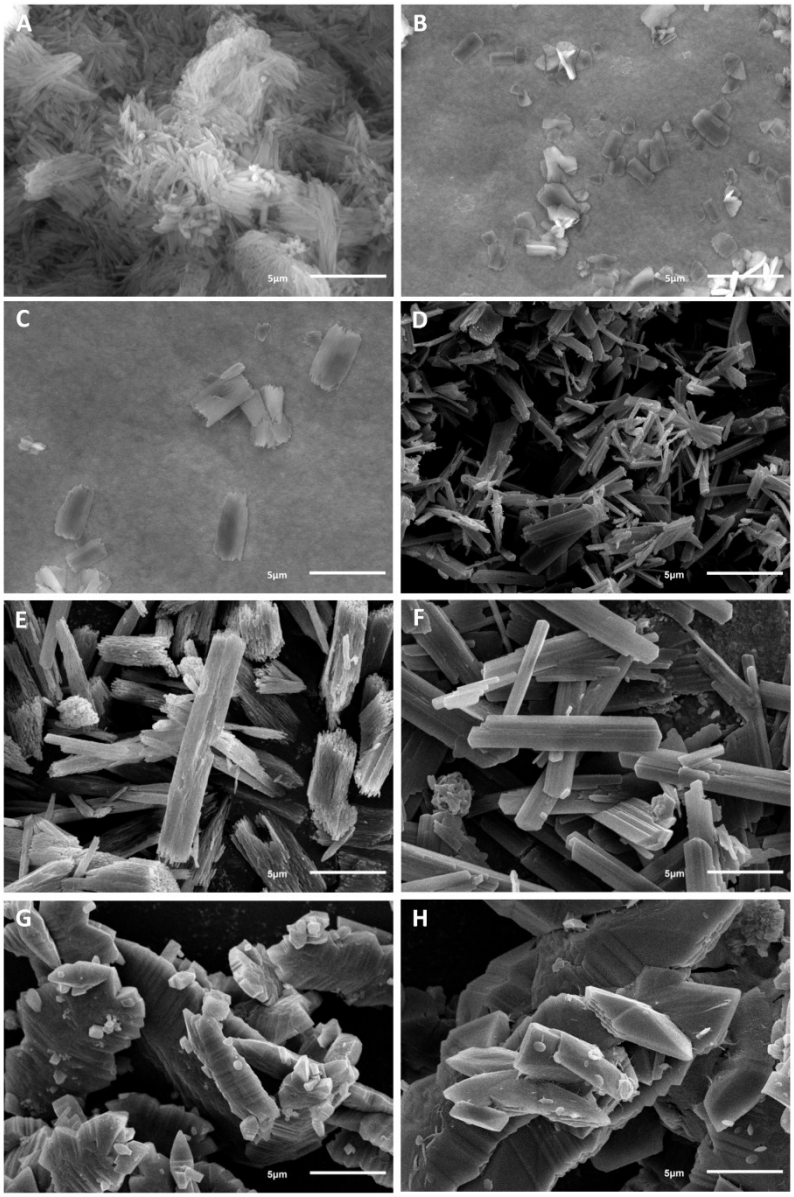

Figure S2. SEM images of MnC_2O_4 resulting from various H_2O/DMF volume ratios: 0:1 (A), 1:100 (B), 1:20 (C), 1:10 (D), 1:4 (E), 1:1 (F), 4:1 (G), and 1:0 (H).

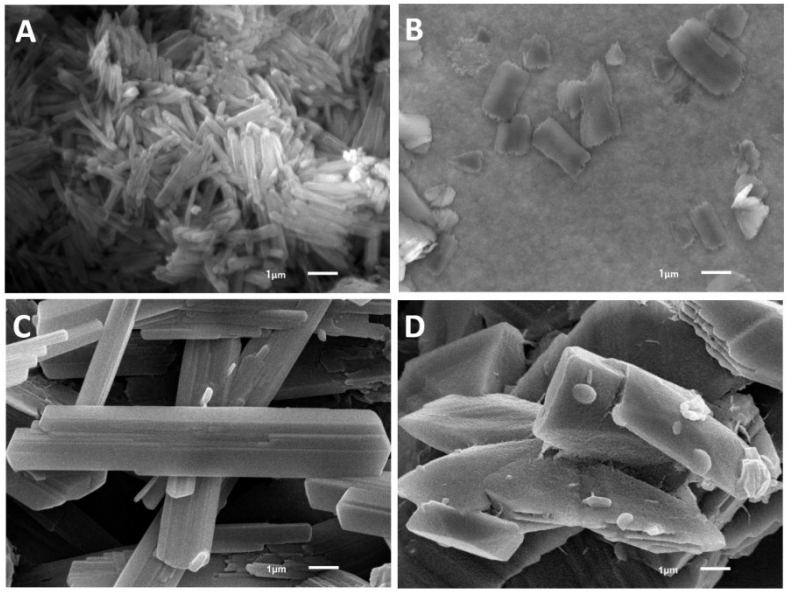

Figure S3. Representative morphology of precursor MnC_2O_4: MR (A), 2D-F (B), MB (C) and IMP (D) resulting from the solution with volume H_2O/DMF ratio being 0:1, 1:100, 1:1 and 1:0, respectively.

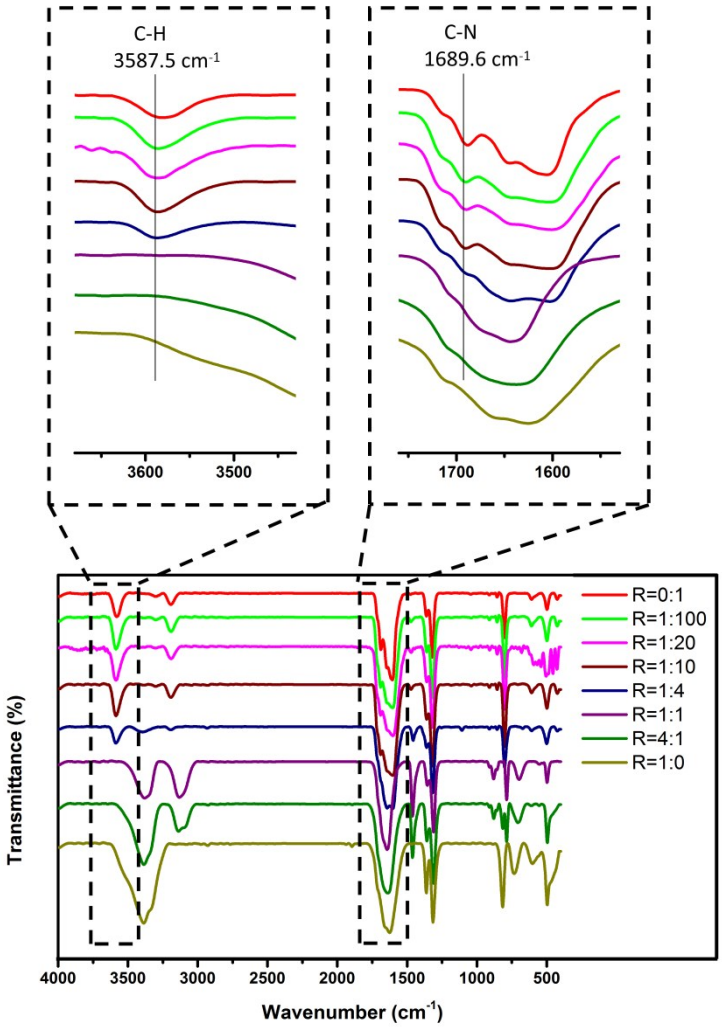

Figure S4. FTIR spectral of precursor MnC_2O_4 resulting from various H_2O/DMF volume ratios.

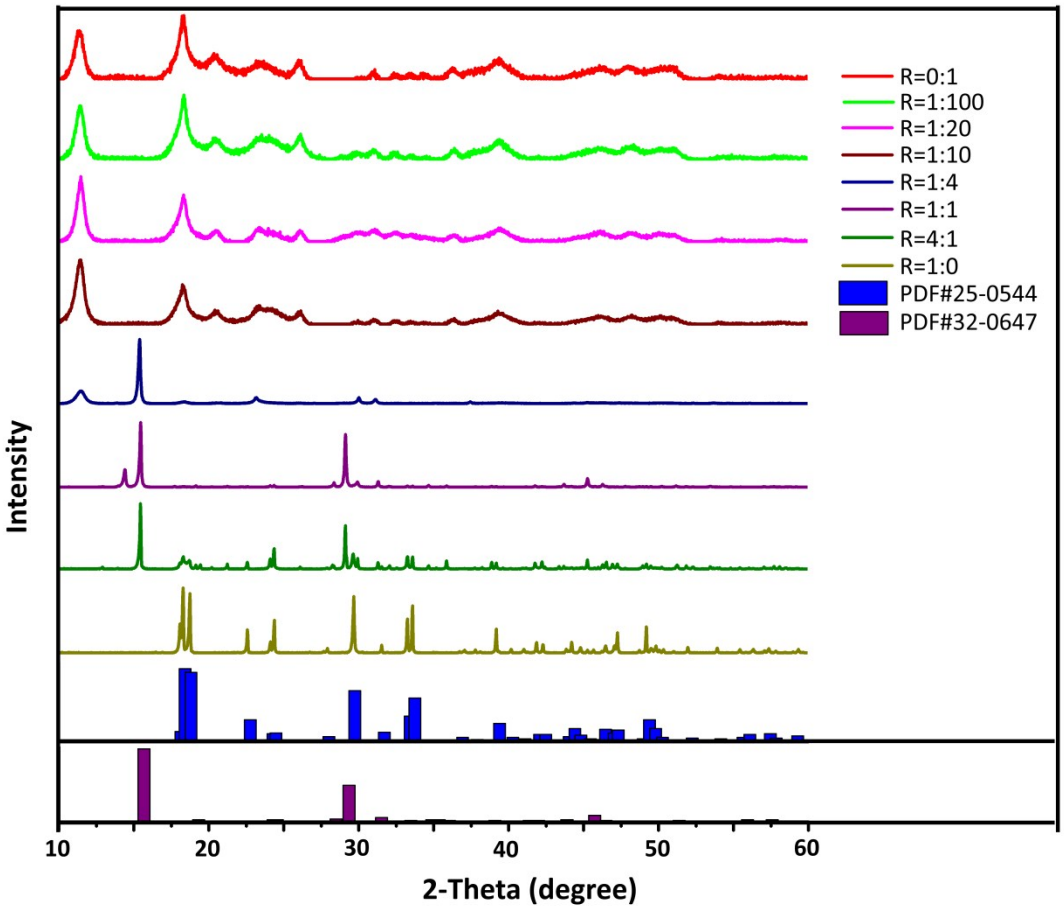

Figure S5. XRD patterns of precursor MnC_2O_4 resulting from various H_2O/DMF volume ratios.

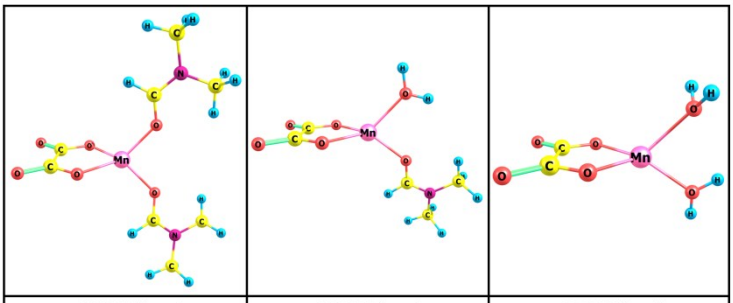

Figure S6. The optimized structures of the precursor nucleus and the corresponding formation energies.

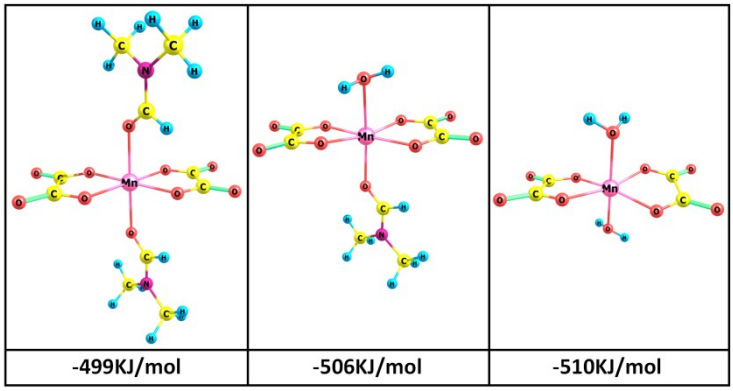

Figure S7. Optimized structure of precursor nucleus after combining with another $C_2O_4^{2-}$ and the corresponding formation energies.

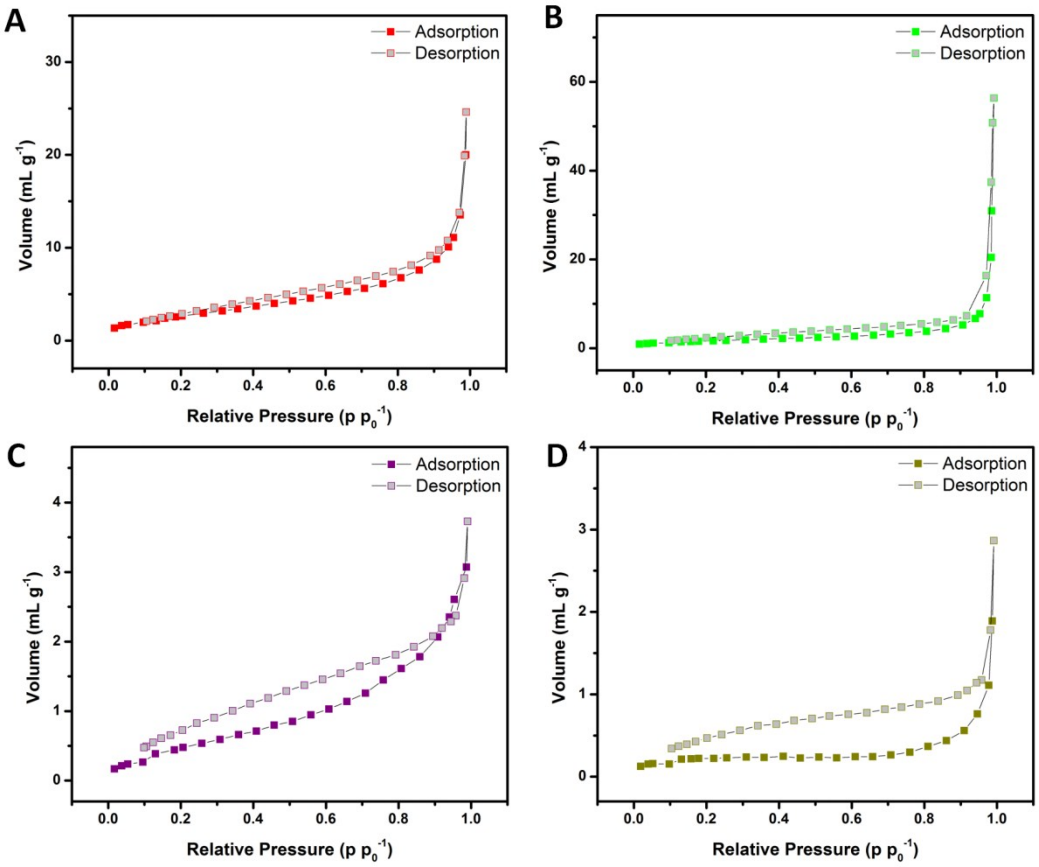

Figure S8. Nitrogen adsorption-desorption isotherms of MnO: NP (A), 2D-F (B), MB (C), and IMP (D).

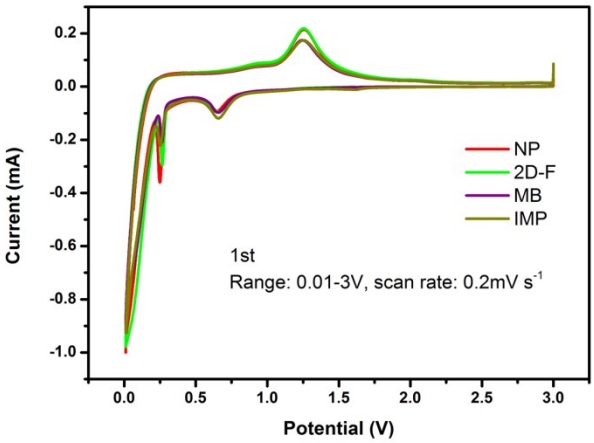

Figure S9. Cyclic voltammograms of four MnO samples.

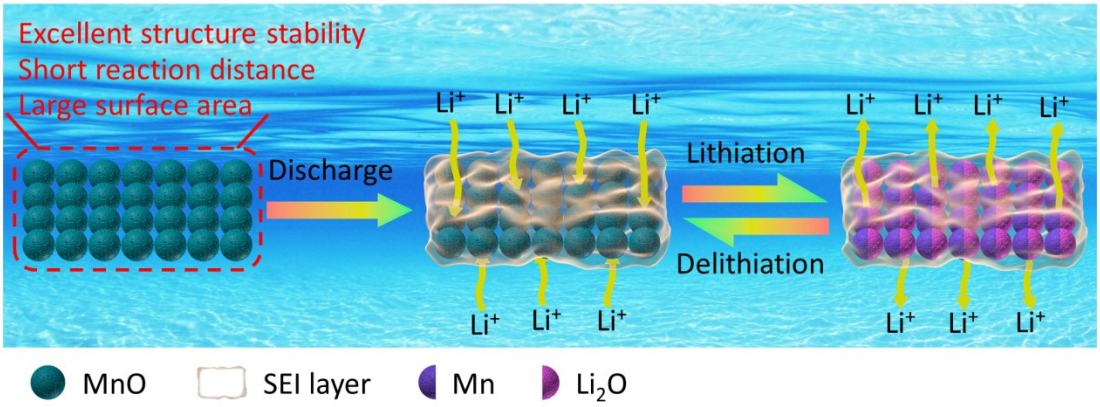

Figure S10. Schematic dimensional stability of 2D-F during lithiation/de-lithiation.

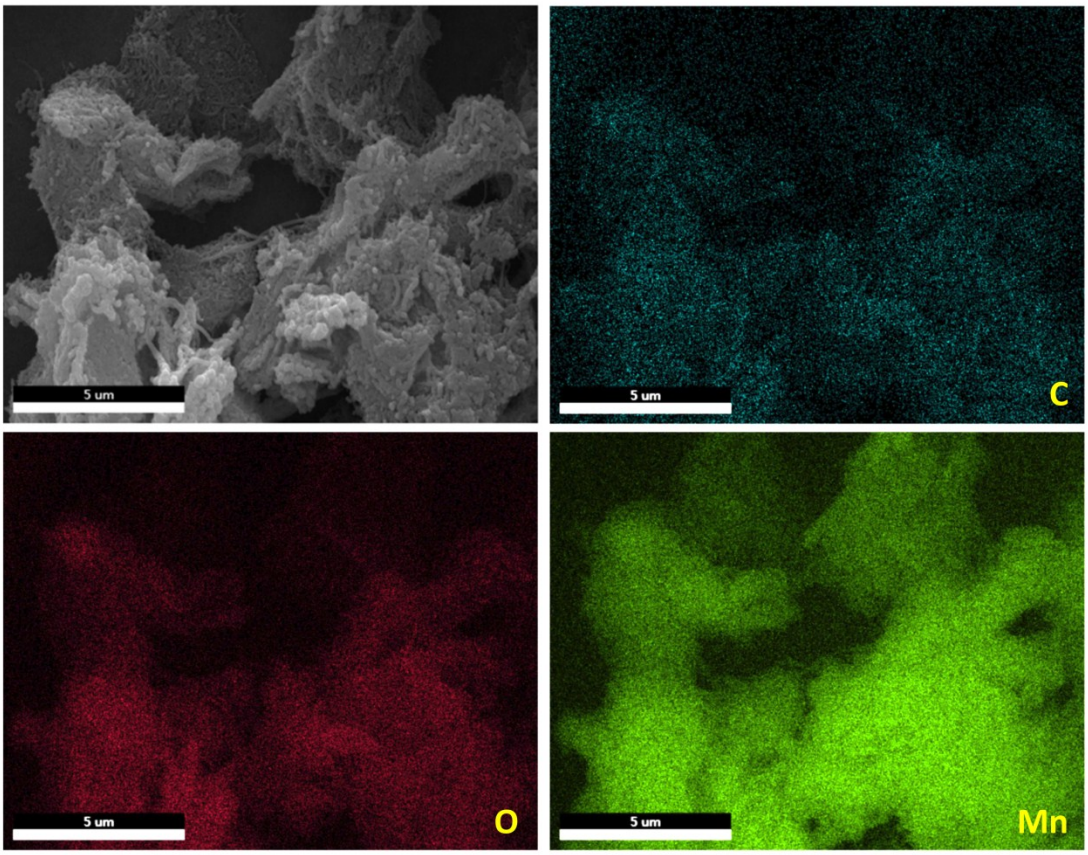

Figure S11. SEM image of 2D-F MnO/CNTs and corresponding EDS elemental mapping of C, O and Mn.

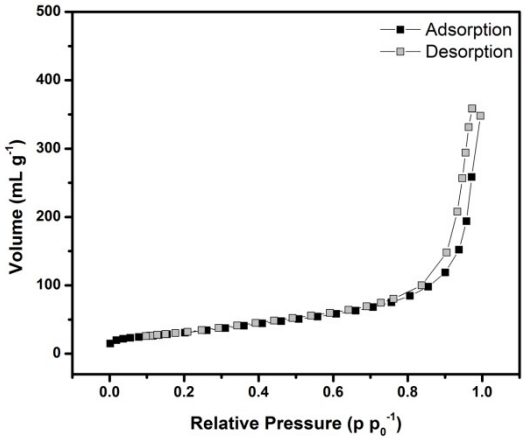

Figure S12. Nitrogen adsorption-desorption isotherms of CNTs.

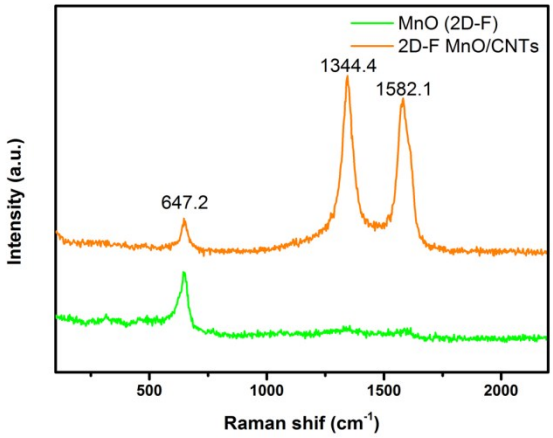

Figure S13. Raman spectra of 2D-F and 2D-F MnO/CNTs.

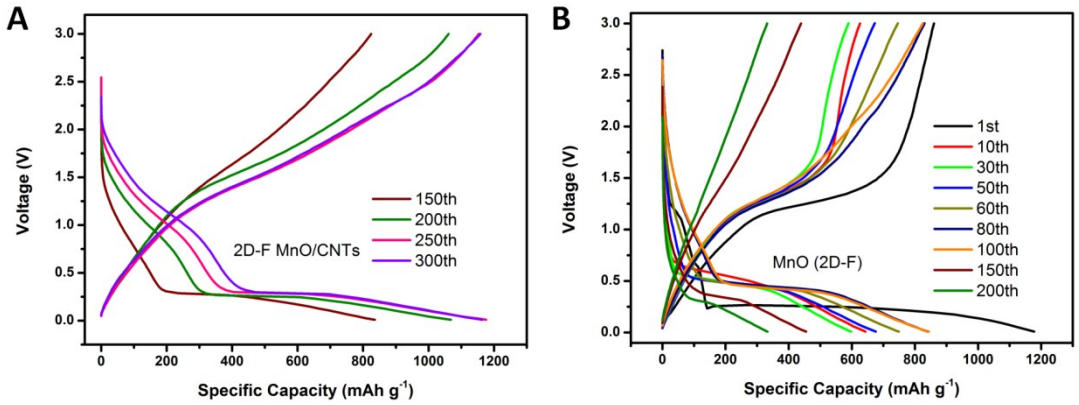

Figure S14. Discharge/charge profiles of 2D-F MnO/CNTs (A) and 2D-F (B) at 0.2 A g^{-1} between 0.01 and 3.00 V.

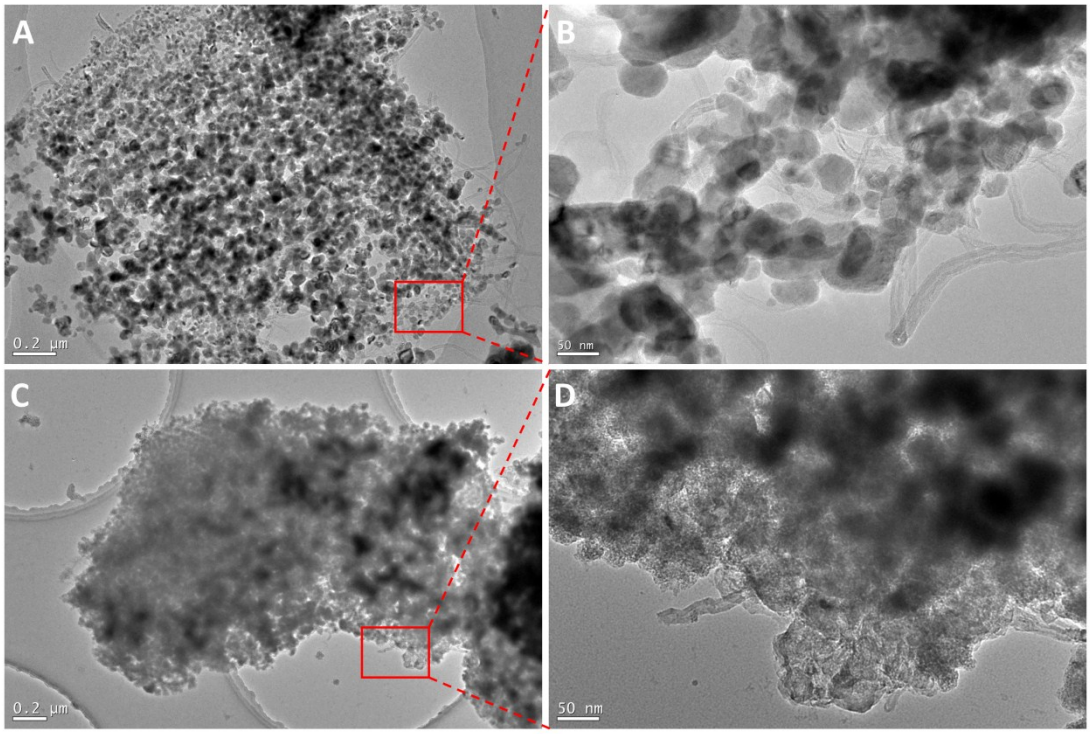

Figure S15. TEM images of 2D-F MnO/CNTs before cycling (A, B) and after 300 cycles (C, D).

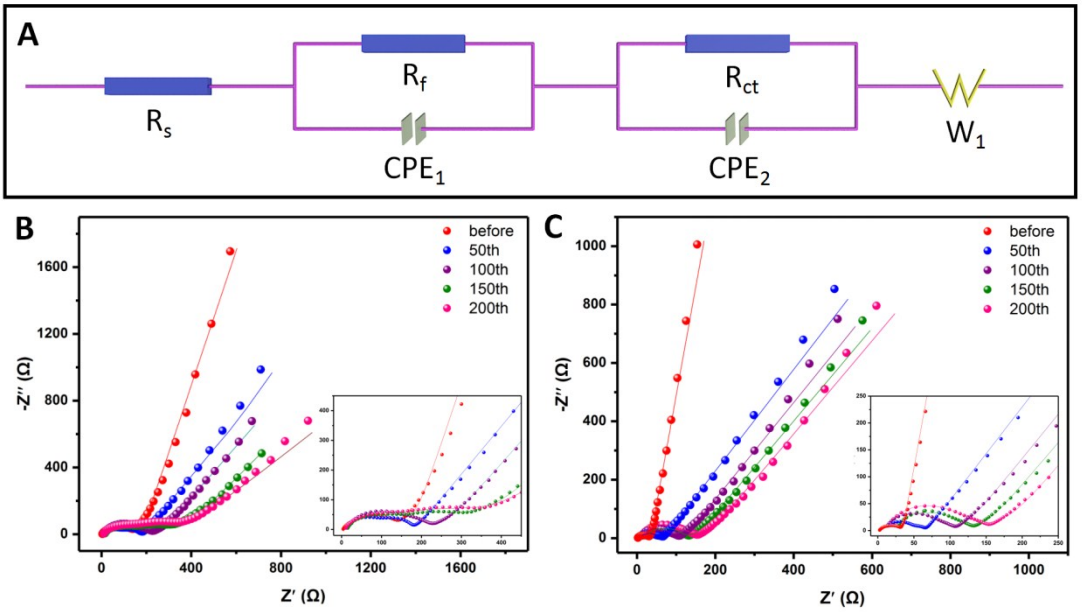

Figure S16. Equivalent circuit (A); Nyquist plots of 2D-F (B) and 2D-F MnO/CNTs (C) before cycling and after various cycle number at 0.2 A g^{-1}, dot lines for experimental data and solid line for fitting.

Table S1. Electrochemical resistance ($R_f + R_{ct}/\Omega$) of 2D-F and 2D-F MnO/CNTs electrodes.

	MnO (2D-F)	2D-F MnO/CNTs
Before	104.0	25.5
50th	175.4	48.8
100th	217.0	83.9
150th	221.8	97.0
200th	273.7	121.4

Table S2. Performance comparison of current work with reported MnO-based materials.

Samples	Current density (mA g^{-1})	Cycle number	Capacity (mAh g^{-1})	Ref
MnO@C core shell nanoplates	200	30	770	[1]
MnO/C nanocomposite	100	100	952	[2]
Mn/C core-shell nanorods	200	40	700	[3]
Porous MnO/C nanotubes	100	100	763	[4]
MnO@C/RGO nanohybrid	380	160	741	[5]
MnO/reduced graphene	100	50	670	[6]
Carbon-coated MnO	50	150	650	[7]
Porous MnO@C microshperes	100	100	525	[8]
Porous MnO/C microspheres	100	100	846	[9]
MnO/C hybrid	300	50	1120	[10]
MnO/GNs nanowires	100	200	815	[11]
MnO@C nanoparticles	200	200	939	[12]
MnO@C microshperes	100	50	702	[13]
Yolk-shell MnO/C nanorod	100	150	649	[14]
MnO Nanocrystals	123	90	923	[15]
2D-F MnO/CNTs	200	300	1158	This work

References

1. X. Zhang, Z. Xing, L. Wang, Y. Zhu, Q. Li, J. Liang, Y. Yu, T. Huang, K. Tang, Y. Qian and X. Shen, *J. Mater. Chem.*, 2012, **22**, 17864.
2. C. Yang, Q. Gao, W. Tian, Y. Tan, T. Zhang, K. Yang and L. Zhu, *J. Mater. Chem. A*, 2014, **2**, 19975-19982.
3. B. Sun, Z. Chen, H.-S. Kim, H. Ahn and G. Wang, *J. Power Sources*, 2011, **196**, 3346-3349.
4. G. L. Xu, Y. F. Xu, H. Sun, F. Fu, X. M. Zheng, L. Huang, J. T. Li, S. H. Yang and S. G. Sun, *Chem. Commun. (Camb)*, 2012, **48**, 8502-8504.
5. D.-H. Liu, H.-Y. Lü, X.-L. Wu, B.-H. Hou, F. Wan, S.-D. Bao, Q. Yan, H.-M. Xie and R.-S. Wang, *J. Mater. Chem. A*, 2015, **3**, 19738-19746.
6. Y. J. Mai, D. Zhang, Y. Q. Qiao, C. D. Gu, X. L. Wang and J. P. Tu, *J. Power Sources*, 2012, **216**, 201-207.
7. K. Zhong, X. Xia, B. Zhang, H. Li, Z. Wang and L. Chen, *J. Power Sources*, 2010, **195**, 3300-3308.
8. S. Guo, G. Lu, S. Qiu, J. Liu, X. Wang, C. He, H. Wei, X. Yan and Z. Guo, *Nano Energy*, 2014, **9**, 41-49.
9. K. Su, C. Wang, H. Nie, Y. Guan, F. Liu and J. Chen, *J. Mater. Chem. A*, 2014, **2**, 10000-10006.
10. D. Sun, Y. Tang, D. Ye, J. Yan, H. Zhou and H. Wang, *ACS Appl. Mater. Interfaces*, 2017, **9**, 5254-5262.
11. Q. Sun, Z. Wang, Z. Zhang, Q. Yu, Y. Qu, J. Zhang, Y. Yu and B. Xiang, *ACS Appl. Mater. Interfaces*, 2016, **8**, 6303-6308.
12. S. Wang, Y. Xing, H. Xu and S. Zhang, *ACS Appl. Mater. Interfaces*, 2014, **6**, 12713-12718.
13. Z. X. Yang Xia, Xiao Dou, Hui Huang, Xianghong Lu, Rongjun Yan, Yongping Gan, Wenjun Zhu, Jiangping Tu, Wenkui Zhang, Xinyong Tao, *ACS Nano*, 2013, **7**, 7083-7092.
14. Z. Cai, L. Xu, M. Yan, C. Han, L. He, K. M. Hercule, C. Niu, Z. Yuan, W. Xu, L. Qu, K. Zhao and L. Mai, *Nano Lett.*, 2015, **15**, 738-744.
15. E. Samuel, H. S. Jo, B. Joshi, S. An, H. G. Park, Y. Il Kim, W. Y. Yoon and S. S. Yoon, *Electrochim. Acta*, 2017, **231**, 582-589.